Supercritical Airfoil Flowfield Measurements

F.X. Hurley,* F.W. Spaid,† and F.W. Roos‡
McDonnell Douglas Corporation, St. Louis, Mo.

and

L.S. Stivers Jr.§ and A. Bandettini¶
NASA Ames Research Center, Moffett Field, Calif.

Detailed measurements in the transonic flowfield about a Whitcomb-type supercritical airfoil profile are presented including surface pressure distributions, far wake surveys, spark schlieren photographs, and a series of vector velocity profiles in the boundary layer and in the near wake. A flowfield composite for the transonic drag rise condition is constructed from these data. The boundary-layer measurements are compared with current correlation and computation schemes, and the importance of viscous thickening effects is demonstrated by the results of wave drag rise calculations for the thickened and unthickened profiles.

Nomenclature

a = function of M_e, γ, and r in van Driest transformation, Eq. (3)
c = airfoil chord
C_d = airfoil section drag coefficient, $C_d = \int C_d' d(z/c)$
C_d' = point section drag coefficient, Eq. (1)
C_l = airfoil section lift coefficient, $C_l = \int (C_{P_L} - C_{P_U})\, d(x/c)$
C_f = local skin friction coefficient, $C_f = \tau/q_e$
C_f^* = skin friction coefficient computed from transformed velocity profile, u^*
C_p = pressure coefficient, $C_p = (P - P_\infty)/q_\infty$
d = probe tip depth
H = boundary-layer shape factor, $H = \delta^*/\theta$
M = freestream Mach number
P = pressure
q = dynamic pressure, $q = \frac{1}{2}\rho u^2$
r = recovery factor
R_{le} = airfoil leading-edge radius
Re_c = Reynolds number based on chord
T = temperature
u = velocity magnitude
u^* = speed transformed by van Driest transformation, Eqs. (3) and (4)
u_τ = shear velocity, $u_\tau = (\tau_w/\rho_w)^{1/2}$
w = empirical wake function, Eq. (5)
x = coordinate measured parallel to freestream direction
y = spanwise coordinate
z = coordinate normal to x-y plane
α = angle of attack
γ = specific heat ratio
δ = boundary-layer thickness, Eq. (5)
δ^* = boundary-layer displacement thickness, $\delta^* = \int_0^r [1 - (\rho u/\rho_e u_e)]\, dz$
θ = boundary-layer momentum thickness, $\theta = \int_0^\delta (\rho u/\rho_e u_e)[1 - (u/u_e)]\, dz$
ν = kinematic viscosity
Π = wake coefficient for transformed boundary-layer profile, Eq. (2)
π = pi, = 3.1459
ρ = density
τ = shear stress

Subscripts

c = based on airfoil chord
e = conditions at edge of boundary layer
le, te = leading edge, trailing edge
r = measured by drag rake
t = total
U, L = upper, lower
w = conditions at the wall (airfoil surface)
∞ = freestream conditions

Submitted August 8, 1974; revision received January 24, 1975, presented as Paper 75-880 at the AIAA 8th Fluid and Plasma Dynamics Conference, Hartford, Connecticut, June 16-18, 1975. This research was conducted under the McDonnell Douglas Independent Research and Development Program in cooperation with the NASA Ames Research Center.

Index categories: Subsonic and Transonic Flow; Jets, Wakes, and Viscid-Inviscid Flow Interactions; Aircraft Aerodynamics.

*Scientist, McDonnell Douglas Research Laboratories. Member AIAA.

†Senior Scientist, McDonnell Douglas Research Laboratories. Associate Fellow, AIAA.

‡Scientist, McDonnell Douglas Research Laboratories. Member AIAA.

§Aerospace Scientist, Aerodynamics Branch, NASA Ames Research Center. Member AIAA.

¶Test Engineer, Experimental Investigations Branch, NASA Ames Research Center.

Introduction

COMPRESSIBILITY drag rise, together with the buffeting phenomenon, limits the Mach-number, lift-coefficient flight envelopes of modern jet aircraft operating in the transonic speed regime. Therefore, airfoil section designs which alleviate or delay the onset of drag rise and buffeting can contribute to higher maximum speeds (transport application) or better maneuvering performance (fighter application).

The Whitcomb NASA supercritical airfoil introduced in 1967[1] demonstrated considerably delayed drag rise in terms of $C_d(M)$, compared with conventional airfoils. Since that time, various profile refinements have been explored and several full-scale flight test programs are in progress. A review of supercritical aerodynamics is given in Ref. 2.

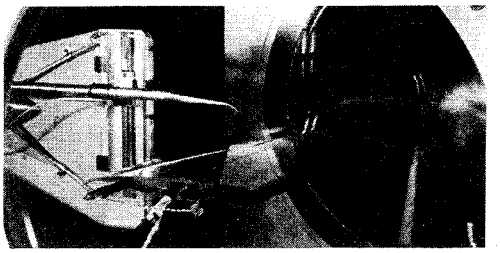

Fig. 1 NASA-Ames two-by-two foot transonic wind tunnel test section with MDRL probe rig and DSMA 523 airfoil model mounted for the test.

Research projects aimed at various specific applications have also been conducted within industry. Efforts by Yoshihara and his co-workers at General Dynamics on powered supercritical profiles are reported in Ref. 3. The McDonnell Douglas Corporation (MDC), McDonnell Aircraft Company (MCAIR) and Douglas Aircraft Company (DAC) have accomplished research on low-moment supercritical profiles[4] and on Whitcomb-type vs conventional profiles,[5] respectively. Typical computer analysis (inviscid) methods are summarized in Refs. 6-8.

Detailed static and dynamic flowfield measurements are presented in Ref. 9. These data correlated the approach and the occurrence of transonic drag rise on a supercritical airfoil with its particular shock system, with apparent trailing-edge separation on the upper and lower surfaces (depending on the value of lift coefficient), and with single point wake fluctuation energy.

It was felt that the mechanisms of the transonic drag rise and buffeting could be better understood if boundary layer and near wake velocity profiles were available, as for example in Ref. 10, in conjunction with the usual surface pressure distributions as well as full flowfield photographs. Also, velocity vector profiles were considered more useful than scalar speed profiles in that they illustrate more clearly the influence of viscous flow development on effective airfoil shape. The ultimate purpose of assembling a detailed picture of the supercritical airfoil flowfield in drag rise is to identify areas for improved design, and to define limits of potential performance improvement. This philosophy also accompanies the data presented in Ref. 11.

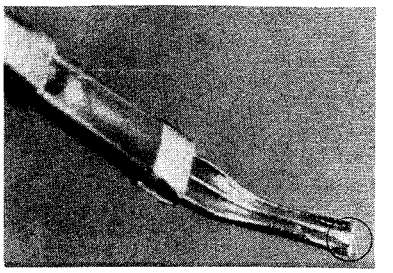

Photograph of probe

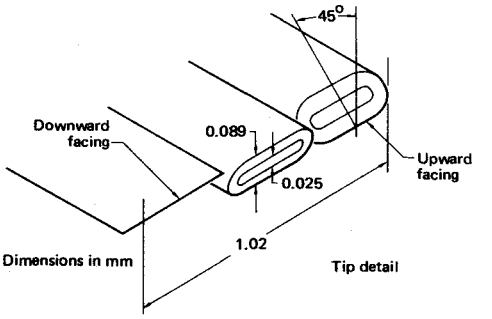

Fig. 2 MDRL triple pressure probe.

The measurements were obtained by McDonnell Douglas Research Laboratories (MDRL) through a cooperative test program with NASA Ames Research Center. Dynamic data acquired during the test series, including surface pressure fluctuations, wake flow unsteadiness, model vibrations, and a study of three-dimensionality effects were reported separately.

Table 1 DSMA 523 profile coordinates

x/c	z_{upper}/c	z_{lower}/c	x/c	z_{upper}/c	z_{lower}/c
0.000500	0.005069	−0.005096	0.460000	0.055146	−0.052143
0.001000	0.007096	−0.007128	0.480000	0.054973	−0.051136
0.002500	0.011063	−0.011078	0.500000	0.054723	−0.049915
0.005000	0.015320	−0.015320	0.520000	0.054390	−0.048483
0.007500	0.018417	−0.018417	0.540000	0.053976	−0.046780
0.010000	0.020716	−0.020671	0.560000	0.053486	−0.044613
0.012500	0.022651	−0.022548	0.580000	0.052917	−0.042006
0.015000	0.024267	−0.024135	0.600000	0.052269	−0.038885
0.020000	0.026918	−0.026744	0.620000	0.051540	−0.035181
0.030000	0.030729	−0.030667	0.640000	0.050726	−0.030940
0.040000	0.033459	−0.033607	0.660000	0.49826	−0.026390
0.060000	0.037407	−0.038087	0.680000	0.048832	−0.021541
0.080000	0.040367	−0.041739	0.700000	0.047725	−0.016958
0.100000	0.042987	−0.044548	0.720000	0.046494	−0.012692
0.120000	0.045198	−0.046796	0.740000	0.045130	−0.008750
0.140000	0.047017	−0.048616	0.760000	0.043625	−0.005200
0.160000	0.048543	−0.050114	0.780000	0.041942	−0.002041
0.180000	0.049828	−0.051348	0.800000	0.040043	(+)0.000686
0.200000	0.050902	−0.052370	0.820000	0.037907	0.002965
0.220000	0.051802	−0.053207	0.840000	0.035502	0.004757
0.240000	0.052563	−0.053890	0.860000	0.032780	0.006021
0.260000	0.053199	−0.054423	0.880000	0.029666	0.006687
0.280000	0.053729	−0.054808	0.900000	0.026155	0.006606
0.300000	0.054161	−0.055056	0.0920000	0.022185	0.005630
0.320000	0.054513	−0.055163	0.940000	0.017708	0.003565
0.340000	0.054788	−0.055137	0.960000	0.012642	(+)0.000348
0.360000	0.054998	−0.054978	0.980000	0.006842	−0.004210
0.380000	0.055149	−0.054701	1.000000	(+)0.000308	−0.010109
0.400000	0.055240	−0.054283			
0.420000	0.055272	−0.053719		$R_{le}/c=0.023$	
0.44000	0.055247	−0.053009			

Facilities and Equipment

These cooperative MDRL-NASA tests were conducted in the NASA Ames Research Center Two-by-Two-Foot Transonic Wind Tunnel. This variable-speed continuous flow, ventilated-wall facility has been re-engineered by NASA for two-dimensional research testing on occasion by the addition of motorized, rotating, thick-glass, model-supporting side windows mounted in solid, plane sidewalls. Based on a 6-in. chord dimension, a Reynolds number of 4×10^6 can be achieved for high subsonic runs. An 82-tube, traversing drag rake, and a spark schlieren camera are available. The point drag coefficient C_d' which is integrated to give C_d is:

$$C_d' = 2(P_{tr}/P_{t\infty})^{(\gamma-1)/\gamma}(P_r/P_\infty)^{1/\gamma} \times \left[\frac{1-(P_r/P_{tr})^{(\gamma-1)/\gamma}}{1-(P_\infty/P_{t\infty})^{(\gamma-1)/\gamma}}\right]^{1/2} \times \left[1-\left[\frac{1-(P_\infty/P_{tr})^{(\gamma-1)/\gamma}}{1-(P_\infty/P_{t\infty})^{(\gamma-1)/\gamma}}\right]^{1/2}\right] \quad (1)$$

Figure 1 shows the tunnel test section with the MDRL provided model and probe rig. Table 1 defines the contour of the DSMA 523 supercritical airfoil section which is essentially that of Ref. 1 with the addition of aft thickening to provide a blunt trailing edge 1% chord thick. The stainless steel model was equipped with 125 static pressure orifices of 0.20 mm diam to establish the chordwise pressure distributions as well as to examine three-dimensionality. A leading-edge transition band was applied, observing the recommendations of Ref. 12. This location was chosen in an attempt to ensure that the boundary layer would always be turbulent upstream of a shock-wave boundary-layer interaction, and thus avoid anomalies in the data arising from interactions between a shock wave and the location of boundary-layer transition. Transition near the leading edge in this Reynolds number range results in somewhat thicker boundary layers than those which would be typical of flight Reynolds numbers. The probe rig was designed to provide fully three-dimensional probe transversing capability. Vertical motion was of high resolution (approximately 0.05 mm between points) for boundary-layer traverses, and both vertical and spanwise motions were remotely controlled and monitored during a run. The pressure probe (Fig. 2) used for the flowfield surveys was a three-tube device utilizing different orifice planes (face angles) to produce pressure triplets that were calibrated against local streamline direction, as in yaw-head probes. The tip depth d was 0.08 mm. Details of fabrication and operation were reported separately.

Results and Discussion

Since the primary purpose of the measurements was to describe the flow about the DSMA 523 supercritical airfoil within its rapid transonic drag rise, most of the present data center on the single condition: $M=0.83$, $C_l=0.54$. This is near the beginning of the speed regime where the drag rises rapidly with increasing Mach number and where the lift coefficient is representative of transport aircraft cruise. Figures 3-6 place this condition in the context of the general performance of the airfoil.

Figure 3 shows the evolution of the flowfield with increasing lift coefficient, for a fixed Mach number $M=0.82$ representing supercritical flow but moderately low drag. It is seen that the positive lift contribution of the rearward camber is maintained over a wide range of conditions; hence, the lower surface develops the greater suction and more severe terminating shock waves at low, positive C_l.

The flowfield evolution with increasing Mach number for a given lift coefficient $C_l=0.51\pm0.03$ is presented in Fig. 4. The upper surface shock wave moves rapidly towards the trailing edge as M increases by only a few hundredths. At M

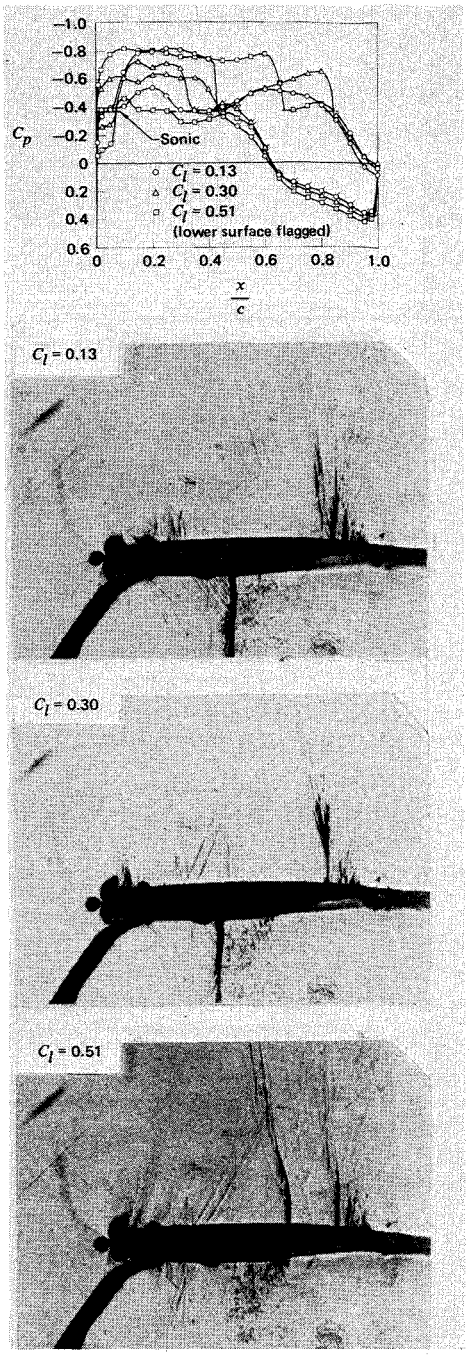

Fig. 3 Development of flowfield and surface pressure distribution with lift coefficient. $M=0.82$, $Re_c=3.0-3.5\times10^6$.

$=0.86$ the shock is strong and extensive and is nearly fixed at a rearward station. The wake is visibly broadened. The schlieren photographs suggest that the lower surface concavity carries a very thick or partly separated boundary layer at all conditions, which reattaches and/or thins down before reaching the trailing edge. It is conceivable to interpret this as only a localized sidewall effect; however, two-dimensional pressure distribution calculations indicate that there is a substantial thickening in the concavity.

Figure 5 shows the development of far wake (drag) profiles with increasing Mach number. The major effect is one of wake broadening, skewed to the upper surface side, suggesting enlarged shock losses there. The data corresponding to $C_l>0.3$ show a roughly constant value of C_d at the lower Mach numbers, with the rapid rise beginning in the vicinity of $M\simeq0.81$.

The drag level in the lower Mach number range is higher than would be computed for the airfoil at subsonic con-

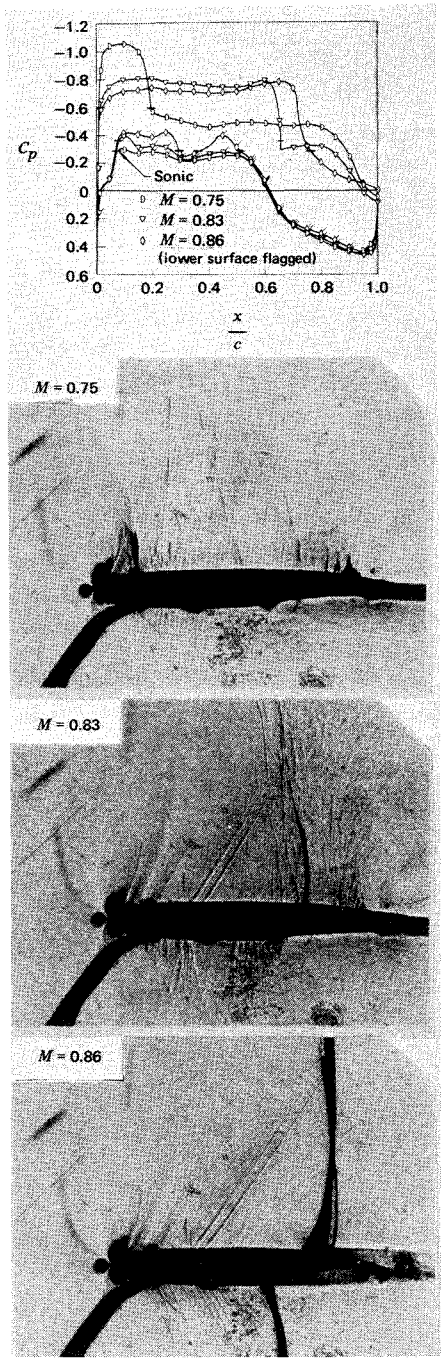

Fig. 4 Development of flowfield and surface pressure distribution with Mach number. $C_l = 0.51 \pm 0.03$, $Re_c = 3.0 - 3.5 \times 10^6$.

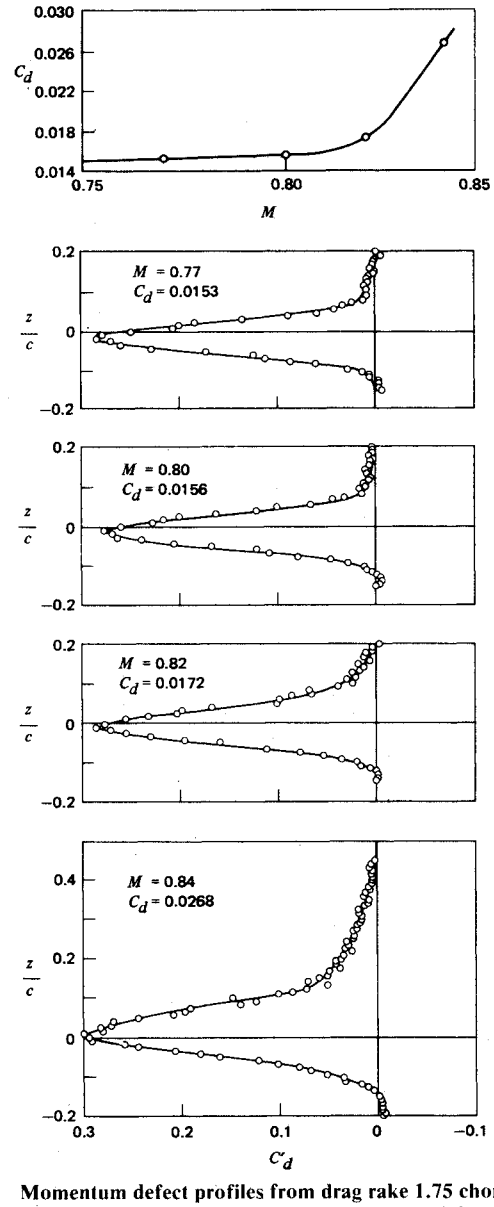

Fig. 5 Momentum defect profiles from drag rake 1.75 chord lengths downstream of trailing edge at $C_l = 0.53 \pm 0.02$, $Re_c = 3.0 \times 10^6$.

ditions, at the test Reynolds number with transition fixed at the leading edge. Upper-surface shocks, which already exist at $M = 0.75$, and a possible separated region on the aft portion of the lower surface are believed to contribute to this drag level. In addition to the schlieren photographs, comparisons between experimental and computed pressure distributions (an example of which will be presented later), and more recent unpublished data indicate that the boundary layer in the lower surface concavity was separated during most of the present series of tests.

In Fig. 6, the evolution of an upper surface, rearward boundary-layer separation with increasing Mach number is shown clearly by the series of trailing-edge velocity vector profiles. As speed increases through $M = 0.83$, the boundary layer thickens, develops an inflection point, and separates with streamlines that diverge markedly from the surface. (The data points indicated by circles rather than by vectors represent velocities too low or too close to the surface to determine directions accurately; also reversed velocities could not be measured.)

The trailing-edge region for $M = 0.83$, $C_l = 0.54$ is mapped by the three vector profiles presented in Fig. 7. The flow is attached to $x/c = 0.95$, and a small amount of separation is indicated at the trailing edge. The near wake is highly asymmetric, as a result of the thick boundary-layer shock losses on the upper surface. The flow inclination angle within the boundary layer does not vary appreciably with vertical location, z/c, but the near wake profile shows a substantial upward component of velocity for $z/c < 0$. Apparently the lower surface streamlines curl upward about the thick trailing edge and its associated dead-water region, thus continuing the expansion that is seen in the last 5% chord of the lower surface pressure distribution.

Figure 8 presents near wake vector profiles for the same flow condition as in Fig. 7. The gradients in speed and inclination angle are observed to be smoothed quite rapidly in this region, so that the flow is nearly parallel at $x/c = 1.5$.

In Fig. 9, the $x/c = 1.05$ profile is plotted in a scalar format, i.e., speed-ratio magnitude and direction, separately. The maximum gradient in flow angularity occurs where the speed is lowest, as is the case, for example, at a free stagnation

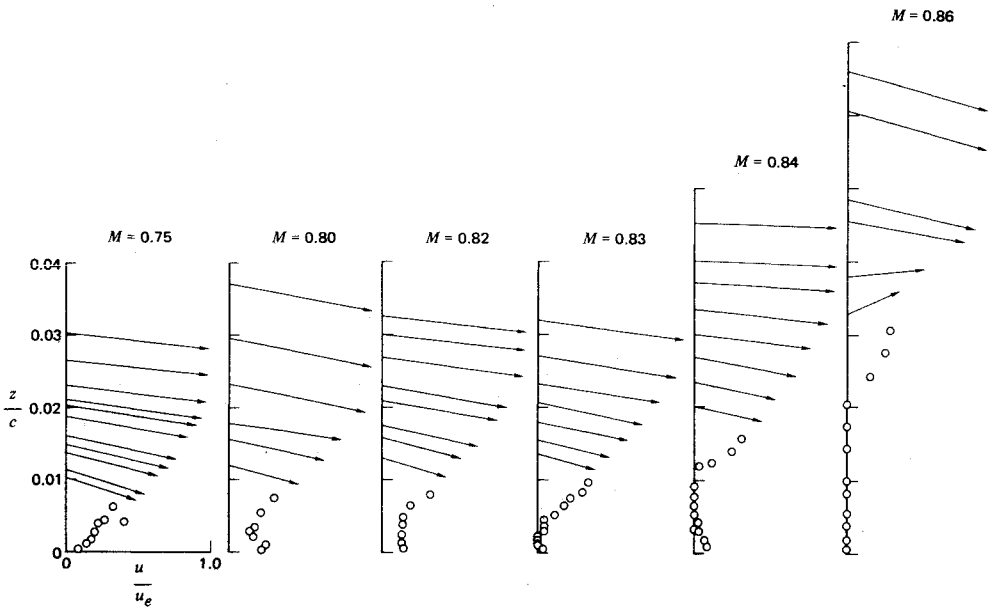

Fig. 6 Influence of Mach number on trailing-edge velocity profiles at $C_f = 0.54 \pm 0.04$, $Re_c = 3.0 \times 10^6$.

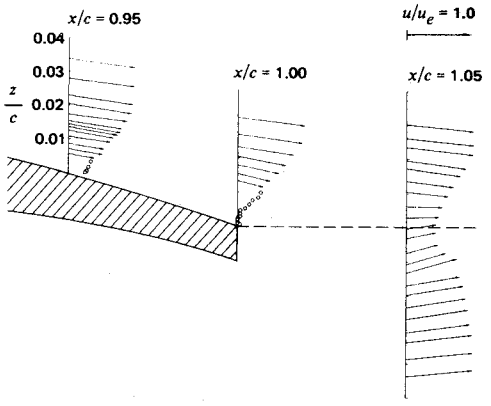

Fig. 7 Velocity profiles near trailing edge at $M = 0.83$, $C_f = 0.54$, $Re_c = 3.0 \times 10^6$.

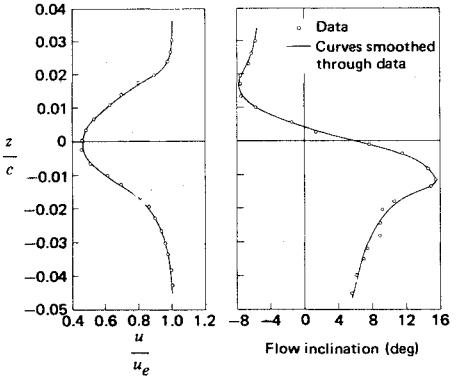

Fig. 9 Near wake speed and flow inclination profiles at $x/c = 1.05$, $M = 0.83$, $C_f = 0.54$, $Re_c = 3.0 \times 10^6$.

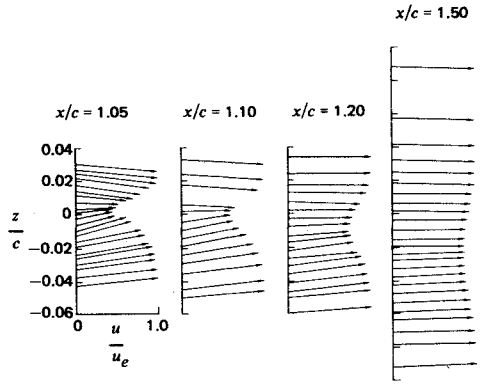

Fig. 8 Evolution of near wake velocity profiles at $M = 0.83$, $C_f = 0.54$, $Re_c = 3.0 \times 10^6$.

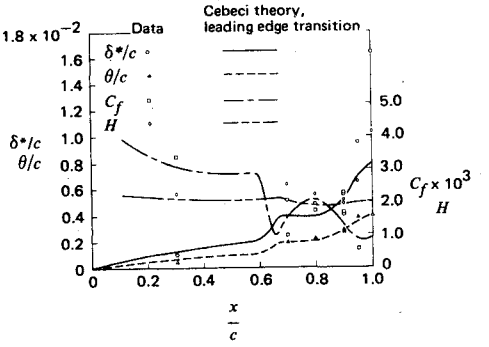

Fig. 10 Comparison of measured and calculated boundary-layer properties at $M = = 0.83$, $C_f = 0.54$, $Re_c = 3.0 \times 10^6$.

(wake closure) point. Such a point must exist further upstream, near the finite thickness trailing edge, even in the absence of any boundary-layer separation.

Figure 10 compares upper surface boundary-layer integral properties and skin friction coefficients measured at $M = 0.83$, $C_f = 0.54$, with calculations obtained from the Cebeci program.[13] The measured pressure distribution was used in the calculation, with the assumption that transition occurred near the leading edge. The measured and calculated values of momentum thickness are in excellent agreement, indicating that leading-edge transition was successfully effected in the experiment. The agreement between the measured and calculated skin friction is also acceptable. However, the calculation does not predict the speed profile accurately near the trailing edge, as illustrated by the lack of agreement between calculated and measured displacement thickness (and shape factor).

Figure 11 presents the upper surface boundary-layer development for the same condition. The turbulent boundary layer experiences considerable thickening both in the shock wave and in the aft recompression, and becomes slightly separated upon reaching the trailing edge. (It is recalled that the upper surface shock is around 64% chord at this condition.) The program predicts the experimental data with

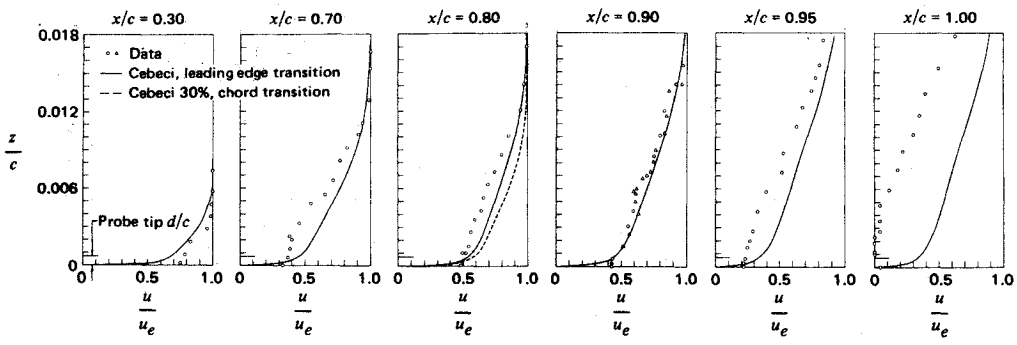

Fig. 11 Boundary-layer speed profile development: experiment vs Cebeci program at $M=0.83$, $C_f=0.54$, $Re_c=3.0\times10^6$.

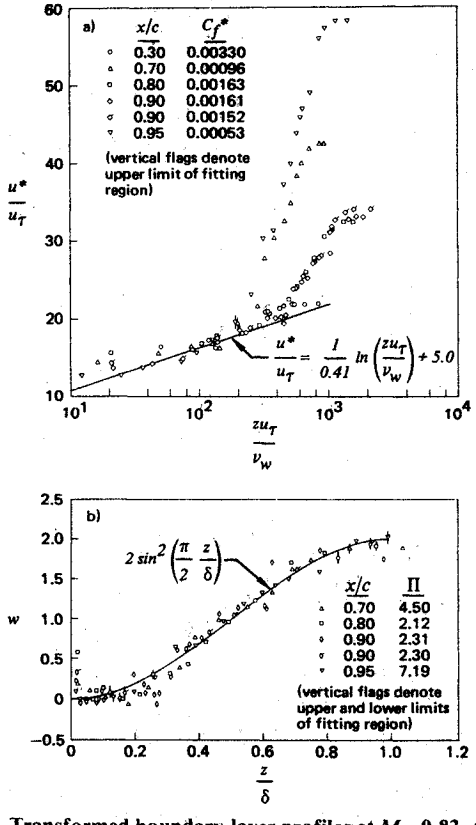

Fig. 12 Transformed boundary-layer profiles at $M=0.83$, $C_f=0.54$, $Re_c=3.0\times10^6$. a) law-of-the-wall coordinates; b) wake components.

reasonable accuracy, except within and just downstream of the sharp pressure rises. The fact that the 80% chord data agrees more closely with the leading-edge transition result than with the 30% transition result indicates that transition occurred well forward of the 30% location. The inclusion of measurements from an extra run in the $x/c=0.90$ chord plot indicates that data repeatibility was good. In these graphs, the probe tip depth $d/c=0.0006$ is shown on the vertical axis.

The $M=0.83$, $C_f=0.54$ boundary-layer data are compared in Fig. 12 with the wall-wake formula of Coles,[14]

$$u^*/u_\tau=(1/0.41)\ln(zu_\tau/\nu)+5.0+(\Pi/0.41)w \tag{2}$$

using the transformation of van Driest,[15]

$$u^*=(u_e/a)\sin^{-1}(au/u_e) \tag{3}$$

where

$$a=\left[\frac{r[(\gamma-1)/2]M_e^2}{1+r[(\gamma-1)/2]M_e^2}\right]^{1/2} \tag{4}$$

The empirical wake function w has been taken as

$$w=2\sin^2(\pi z/2\delta) \tag{5}$$

The parameters δ (scaling/boundary-layer thickness), u_τ (skin friction) and Π (wake proportion) have been determined by a least-squares fitting process. The data of Fig. 12a obtained nearest the wall are seen to lie significantly above the universal curve. This behavior is interpreted as an indication of model surface interference with the pitot-pressure measurement. Although significant scatter is present, a logarithmic region can be observed for each of the data sets. The data obtained at the most forward station on the airfoil, $x/c=0.3$, show the deviation from a straight line, i.e., the wake component, to be negligible, a characteristic of boundary layers associated with low Reynolds numbers or favorable pressure gradients.[14] Each of the other data sets shows substantial wake components. The data of Fig. 12b, from which the law-of-the-wall component has been subtracted, are in good agreement with Coles' empirical wake function. Large values of the wake coefficient Π in this representation correspond to large deviations from the logarithmic law in the previous representation; i.e., to boundary layers approaching separation. The largest values are obtained just downstream of the shock, at $x/c=0.7$, and near the trailing edge.

From these data it can be concluded that the DSMA 523 profile in its rapid transonic drag rise undergoes a type B separation, as defined by Pearcey et al.[16] That is, there is a trailing-edge stall which is not part of a full separation (without reattachment) from the upstream shock wave. There may be a small bubble at the base of the shock, but the boundary layer does reattach and is undergoing rehabilitation before the compression near the trailing edge causes it to separate. The subsonic, nearly constant pressure region of recovery just downstream of the shock wave becomes shorter as the Mach number is increased and the shock wave moves rearward. As a result, increasing M enlarges the extent of the trailing-edge separation.

Figure 13 is a composite of the vector velocity flowfield in the trailing-edge region for the condition $M=0.83$, $C_f=0.54$ (note that the vertical scale has been stretched). Speed profiles have been plotted, together with selected velocity vectors, all normalized by the freestream speed. Also included are values of displacement thickness, values of δ (obtained, as explained, from the wall-wake fitting process), and streamlines computed from integrals of mass flux beginning at the wall. (A systematic discrepancy of 3.8° between flow inclination angles measured by the probe and streamline directions obtained from integrals of mass flux was adjusted in favor of the latter; instrumentation misalignment under probe and rig aerodynamic loading was judged to be the likely source of the disagreement.)

Figure 13 illustrates in a more graphic fashion some of the trends discussed earlier, including the thickened boundary layer at 70% chord (downstream of the shock), its subsequent recovery, and its further thickening and start of separation in

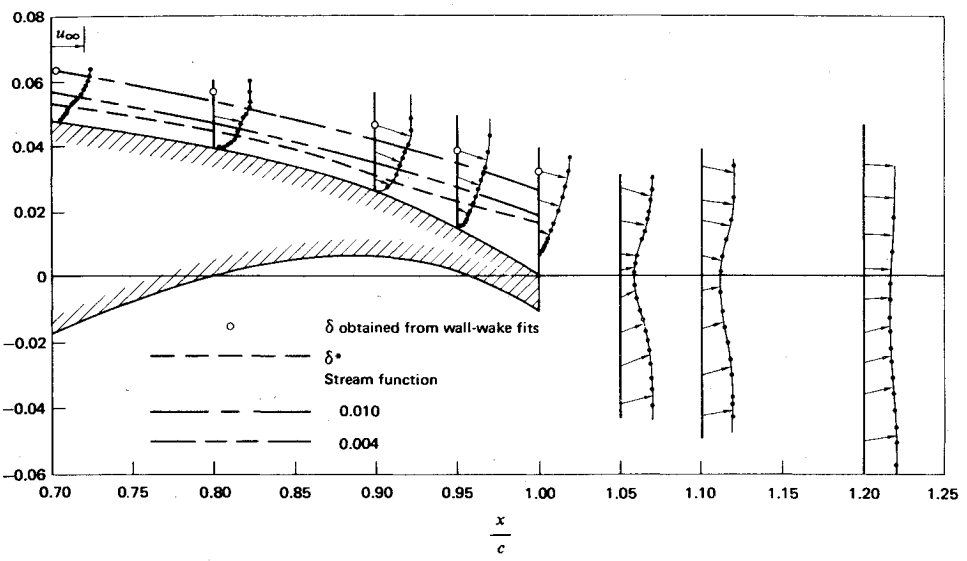

Fig. 13 Flowfield details near trailing edge at $M=0.83$, $C_\ell=0.54$, $Re_c=3.0\times10^6$.

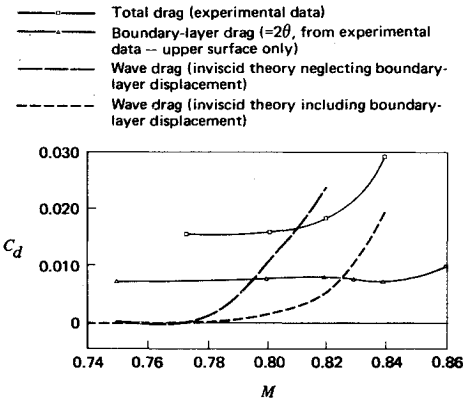

Fig. 14 Drag rise characteristics at $C_\ell=0.54\pm0.01$, $Re_c=3.0\times10^6$.

the last 10% of chord. Both the streamlines and the δ^* distribution are approximately parallel to the airfoil surface for $x/c<0.9$, but the rapid increase in δ^* near the trailing edge causes an effective reduction in aft camber.

The wake is convected downward and spreads rapidly with increasing downstream distance. As previously noted, substantial upward inclination of the flow is observed for $z/c<0$. The region of upward inclination extends substantially below the viscous layer and is still prominent at $x/c=1.2$.

It seems clear that this supercritical airfoil, within its transonic drag rise, has an effective contour at rearward stations which is greatly influenced by boundary-layer/wake behavior. That is, the outer streamlines flow about a shape which is rather different from the airfoil profile.

The Caughey program[8] has been used to compute transonic pressure distributions for the DSMA 523 airfoil with and without the addition of the measured δ^* distribution. The results are as expected; if the displacement effect is omitted, the camber is larger than its effective value at rearward stations, and the upper surface develops too much suction, and stronger, more rearward shock waves than are measured.

These calculations do yield wave drag estimates, and Fig. 14 presents computed and experimental results within the transonic drag rise regime. One conclusion from Fig. 14 is that the changes (with Mach number) in viscous dissipation within the boundary layer are not sufficient to explain the transonic drag rise. Instead, the program with boundary-layer correction predicts a wave drag increase on the airfoil that compares well with the experiment. The computation of drag on the airfoil without the boundary layer compares poorly with the experiment, showing a much earlier drag increase than was measured. This disagreement is consistant with the surface pressure distribution results; unless the boundary layer is included in the airfoil profile definition, the calculation predicts stronger, drag-producing shock waves.

Since the present airfoil was (in effect) designed with a boundary layer included, namely by iterative experiments in a wind tunnel, it should not be surprising that this profile and its performance are de-optimized by the mathematical removal of the boundary layer. (At the high Mach numbers, however, the boundary layer separates drastically from the upper surface, as in Fig. 6, and this separation certainly contributes to the drag increase.)

Conclusions

Flowfield measurements have been presented in the interests of enhancing the understanding of supercritical airfoils and contributing to further design improvements in the future. As with other profiles, the rapid transonic drag rise is accompanied by a variety of shock-wave patterns as well as by a boundary-layer separation, depending on the C_ℓ range being considered. Specifically, the condition of C_ℓ near 0.54 and M equal to 0.83 or greater results in a substantial, rearward upper surface shock wave which aggravates a type-B trailing-edge separation. Streamlines from the lower surface curve sharply upwards to enclose the deadwater region produced by this separation and by the trailing-edge bluntness.

It is necessary to model viscous effects correctly in order to obtain acceptably accurate finite-difference program calculations. Transonic boundary-layer computations match the data results as long as rapid compressions are all downstream or far upstream of the station considered. Measured boundary-layer profiles conform well with combined law-of-wall and law-of-wake functions.

Further research in the following areas is recommended: probe the lower surface concavity flowfield; recontour the upper surface with a view toward delaying or alleviating the rapid drag rise; and investigate the degree to which data obtained in the Reynolds number range of the present experiments are representative of flight conditions.

References

[1] Whitcomb, R.T., "Review of NASA Supercritical Airfoils," ICAS Paper No. 74-10, presented at the 9th Congress of the Intl. Council of Aeron. Sci., Haifa, Israel, Aug. 25-30, 1974.

[2] Ayers, T.G., "Supercritical Aerodynamics Worthwhile over a Range of Speeds," *Astronautics & Aeronautics*, Vol. 10, Aug. 1972, pp. 32-36.

[3] Yoshihara, H., Casten, W.V., Fatta, G.J., Magnus, R.J., and Murray, R.T., "Aeronautical Exploratory Research on Advanced Jet Flap Supercritical Airfoils," General Dynamics/Convair Interim

Tech. Rept. 3/71-2/72, AD744036, Feb. 1972, General Dynamics, San Diego, Calif.

[4]Tranen, T.L., "Rapid Computer Aided Transonic Airfoil Design Method," AIAA Paper 74-501, Palo Alto, Calif., June 1974.

[5]Sewell, A., "The Results of Two-Dimensional Airfoil Tests Conducted in the Ames Six-Foot Wind Tunnel during 1969 and 1970," MDC J5056, May 1973, McDonnell Douglas Corp., Long Beach, Calif.

[6]Krupp, J.A. and Murman, E.M., "Computation of Transonic Flows Past Lifting Airfoils and Slender Bodies," *AIAA Journal,* Vol. 10, July 1972, pp. 880-886.

[7]Garabedian, P.R. and Korn, D.G., "Analysis of Transonic Airfoils," *Communications on Pure and Applied Mathematics, Vol. 24, Nov. 1971, pp. 841-851.*

[8]Caughey, D.A., "Users' Guide to CPROX: A Transonic Airfoil Analysis Program," MDC Q0506, Dec. 1973, McDonnell Douglas Corporation, St. Louis, Mo.

[9]Hurley, F.X. and Roos, F.W., Experimental Study of the Flow Field about an Advanced Transonic Airfoil," MDC Q0479, Dec. 1973, McDonnell Douglas Corporation, St. Louis, Mo.

[10]Cook, T.A., "Measurements of the Boundary Layer and Wake of Two Aerofoil Sections at High Reynolds Numbers and High-Subsonic Mach Numbers," RAE Tech. Rept. 71127, June 1971, Royal Aircraft Establishment, Farnborough, England.

[11]Evans, W., MacKenzie, D., and Romanowski, R., "The Design, Test, and Evaluation of Shockless Transonic Airfoils," U.S. Navy Final Report, Sept. 1973, Contract No. N00019-72-C-03580, Grumman Aerospace Corp., Bethpage, N.Y.

[12]Braslow, A.L., Hicks, R.M., and Harris, R.V., Jr., "Use of Grit-Type Boundary-Layer Transition Trips on Wind-Tunnel Models," TN D-3579, 1966, NASA.

[13]Cebeci, T., Smith, A.M.O., and Wang, L.C., "A Finite Difference Method for Calculating Compressible Laminar and Turbulent Boundary Layers," DAC 67131, March 1969, McDonnell Douglas Corp., Long Beach, Calif.

[14]Coles, D.E., "The Young Person's Guide to the Data," *Proceedings: Computation of Turbulent Boundary Layers, 1968 AFOSR-IFP-Stanford Conference,* Vol. II; Compiled Data, edited by D.E. Coles and E.A. Hirst, Stanford University, Stanford, Calif., 1969.

[15]van Driest, E.R., "Turbulent Boundary Layer in Compressible Fluids," *Journal of the Aeronautical Sciences,* Vol. 18, March 1951, pp. 145-160.

[16]Pearcey, H.H., Osborne, J., and Haines, A.B., "The Interaction between Local Effects at the Shock and Rear Separation—A Source of Significant Scale Effects in Wind-Tunnel Tests on Aerofoils and Wings," *Proceedings of the AGARD Conference on Transonic Aerodynamics,* AGARD-CP-35, Sept. 1968.